ORIGINAL ARTICLE

Dissolution and regeneration of cellulose from N-methylmorpholine N-oxide and fabrication of nanofibrillated cellulose

Nahla El-Wakil[1] · Mohamed Taha[2] · Ragab Abouzeid[1,3] · Alain dufresne[3]

Abstract

Cellulose II nanofibers (R-CNFs) were isolated from Egyptian bleached bagasse pulp fibers via dissolution in N-methyl-morpholine N-oxide (NMMO) and regeneration. The quality and features of the R-CNFs suspension were optically and morphologically characterized and compared to those obtained from two conventional CNFs prepared from pretreated native cellulose (enzymatic hydrolysis (E-CNFs) and TEMPO oxidation (T-CNFs)) isolated from the same cellulosic pulp. Optical microscopy images show the effectiveness of nanofibrillation for all samples with few residual fragments and the absence of macrofibers. The grinding process of R-CNFs results in the formation of CNFs in nanometer scale, as confirmed by AFM and TEM studies. Moreover, the nanopapers prepared from R-CNFs showed mechanical properties (tear resistance and Young's modulus), porosity, and water vapor permeability comparable to those obtained for E-CNFs and T-CNFs. However, R-CNFs suspensions exhibited a lower optical transmittance value (7.5%) and a higher turbidity (315 NTU) against 12.5%, 272 NTU and 25%, 160 NTU for E-CNFs and T-CNFs, respectively ascribed to some CNFs aggregates. The quality index for E-CNFs and T-CNFs was 74.2 and 85.5, respectively, whereas it was only 68.3 for R-CNFs due to the presence of these few fibrillar aggregates after regeneration and fibrillation.

Keywords Regenerated cellulose nanofibers · NMMO solvent · TEMPO-mediated oxidation · Enzymatic treatment · Quality index

1 Introduction

Agricultural wastes, forests, woody crops, and grasses are the main components of biomass, which can offer a promising substitute for petroleum-based sources in many applications. The interference and complexity of the fibrous structure hinder their use in advanced recent applications [1]. Lignocellulosic biomass are the most available renewable feedstock for various applications that can fulfil the requirements for achieving environmentally friendly, biocompatible, and relatively low-cost alternatives to petroleum-based products if processed in the appropriate manner [2, 3]. Nanotechnology played a role in this challenge by making nanocellulose out of the most common biopolymer on earth (cellulose). Extensive research has been devoted in the last few decades to cellulose nanoparticles specially CNFs due to their low density, high strength, and accessibility to modification [4–7]. Composites, cosmetics, paperboard, and medical and pharmaceutical accessories are among the various applications of CNFs [8]. Mechanical disintegration of cellulosic fibers using a highly intense shearing procedure is the commonly used protocol to produce CNFs of width less than 10 nm and several microns in length [9–12]. High energy consumption is the basic characteristic of CNFs production process, as many cycles are required for better defibrillation, whether ultrafine grinding [13], high-pressure microfluidization [14], high-intensity sonication [15], or cryocrushing method is used [16]. For that reason, researchers have joined two or more treatments to ease the fibrillation

✉ Ragab Abouzeid
r_abouzeid2002@yahoo.com

✉ Alain dufresne
alain.dufresne@pagora.grenoble-inp.fr

1 Cellulose and Paper Department, National Research Centre, 33 El-Buhouth Street, Dokki, Giza 12622, Egypt

2 Mechanical Engineering Department, College of Engineering and Technology, Arab Academy of Science, Technology and Maritime Transport, Sadat Road, P.O. Box 11, Aswan, Egypt

3 Univ. Grenoble Alpes, CNRS, Grenoble INP, LGP2, F-38000 Grenoble, France

process and consequently reduce the energy consumption [8]. Also, in this context, a variety of biological [17] and chemical [18] pretreatments have been proposed to enhance cellulosic fibers' fibrillation while keeping the interaction sites and suspension quality. Selective cellulose hydrolysis, supported by an environmentally friendly and low-cost process, is an integrated process achieved by endoglucanase enzymes hydrolysis as a pretreatment step prior to mechanical refining and high-pressure homogenization. However, the resulting fibrils have a larger average diameter and a heterogeneous size distribution, while the branched fibrils are partially fibrillated [19, 20]. Chemical pretreatment can also act as an assistant factor to minimize the fibrillation energy where 2,2,6,6-tetramethylpiperidine-1-oxyl radical-mediated oxidation (TEMPO) is used heavily. The hydroxyl group at carbon 6 of the repeated glucose unit is selectively oxidized to carboxylic group [21]. Due to the repulsive forces of the carboxylate groups, the nanofibrils are separated easily resulting in a colloidal suspension of high stability. The TEMPO-CNFs possess fibrils' length in the range of 800 nm; yet TEMPO is toxic that restricts its use in some applications [22]. Other pretreatments used to obtain various CNFs are summarized elsewhere [23, 24]. Among the techniques reported for nanofibers formation, electrospinning is considered one of the most important techniques [25]. Summing up, the production of CNFs of high quality with cheap, energy-efficient, and non-pollutant process is the challenge of researchers and industry for large scale production. Regardless the mechanical fibrillation stage and whatever its type, the preliminary pretreatment is a decisive step for energy consumption. Cellulose dissolution and regeneration can construct cellulose chains possessing high functionality and offer materials with a wide range of properties to construct fabulous nanofibrous structures [26]. Among the reported cellulose dissolution technologies, an environmentally friendly method based on N-methylmorpholine-N oxide (NMMO) known as Lyocell technology is widely used in the textile industry. In addition to textile, cellulose/NMMO solution can be used to make nanoparticles [27, 28], thin films [29], membranes [30], and aerogels [31]. Oxidation of the hydroxyl groups into onic acids in addition to degradation are the main changes in cellulose during dissolution in NMMO [32]. The content of ionized carboxylic groups and their allocation affect the properties and consistency of the regenerated cellulose [33]. From an economic point of view, solvent recovery is a key factor that determines the feasibility of the used solvent [34]. Recycled NMMO has demonstrated its efficiency with the same activity for the treatment of bleached bagasse pulp [35]. Minimal degradation and ease of recycling were reported in producing Lyocell fibers production process; the solvent recovery was 99.5% [36]. Moreover, deep eutectic solvents have been used for dissolution and regeneration of birch cellulose pulp

[37], ramie fibers [38], and bleached birch Kraft paper [39] for the production of CNFs. Transformation of cellulose II from cellulose I was assessed by Zimmermann et al. (2016) due to cellulose dissolution and regeneration [33].

The novelty in our approach is to prepare the CNFs from regenerated cellulose using the NMMO solvent and compare the morphology, crystallinity, and quality index with the widely used CNFs (E-CNFs and T-CNFs). CNFs with comparable quality to the most extensively used E-CNFs and T-CNFs were formed by regenerating cellulose from a safe and readily recoverable NMMO solvent and then disintegrating it. In this study, the objective was to prepare and analyze a new form of eco-friendly and nanosized diameter R-CNFs and compare them with two established types of CNFs based on TEMPO and enzymatic hydrolysis pretreatments prepared from the same bleached bagasse pulp. The quality index and its related criteria were taken as a parameter of comparison.

2 Experimental

2.1 Materials

Bleached bagasse pulp was kindly provided by Qena Paper Industry Company, Egypt. The bleaching procedure, which is separated into three steps, uses chlorine dioxide, oxygen delignification, and other chlorine dioxide step. The chemical composition of bagasse pulp was 71% a-cellulose, 30% pentosans, 0.8% ash, and a degree of polymerization (DP) of 1200. TEMPO, sodium bromide (NaBr), sodium hypochlorite (NaClO), sodium hydroxide (NaOH), hydrochloric acid (HCl), N-methylmorpholine-N-oxide (NMMO) solution (NMMO/water ratio 50/50), and propyl gallate (PG) were purchased from Sigma Aldrich. Enzyme solution Fiber-Care© R (Novozyme, Denmark) with an endoglucanase activity of 4770 ECU/g was supplied by Arjowiggins, France. Additional chemicals needed for the different analytical methods were also purchased from Sigma-Aldrich. All chemical reagents were used with no further purification.

2.2 Methods

2.2.1 Dissolution of cellulose pulp using NMMO solution

A mixture of NMMO/water (50/50) was used to dissolve the cellulosic material. According to a previous work [40], 3% cellulose concentration based on NMMO concentration was selected to perform the experiment. The dissolution process was carried out at 95 °C and 6.7 kPa, until a clear and homogeneous solution of half the original solution was obtained. The cellulose solution was coagulated in deionized water at 0 °C, and the fibers were then rinsed in deionized water for

around 48 h to remove any residual NMMO and then dried under vacuum for 24 h at 50 °C [33].

2.2.2 Enzymatic treatment of cellulose fibers

Enzymatic hydrolysis was performed using cellulase Celluclast 1.5 L and endoglucanase FiberCare R enzyme solution (with an activity of 4770 ECU/g of solution) with an enzyme concentration of 300 ECU/g of cellulose, as described by Gabriel et al. [41]. About 2 wt. percent cellulose suspensions were incubated with the enzyme for 2 h at 50 °C in a 50 mM acetate buffer solution with a pH of 5. The enzyme activity was inhibited by heating the solution to 80 °C for 20 min and using chloroform (0.01 wt. percent) as a biocide.

2.2.3 TEMPO oxidized cellulose nanofibers

The synthesis of surface-functionalized CNFs by TEMPO-assisted oxidation of cellulose fibers was achieved according to the procedure described by Saito and co-workers [42]. About 10 g of cellulose fibers were suspended in 750 mL of water containing 0.025 g TEMPO and 0.25 g NaBr. NaClO solution (3.84 mmol/g of cellulose) was then added to the slurry under continuous agitation. The pH of the suspension was kept constant at 10.5 at room temperature using NaOH (0.5 N). Finally, the reaction was then stopped, and the pH was adjusted to neutral using HCl. The pulp obtained was washed using deionized water and finally subjected to homogenization to produce functionalized CNFs containing carboxylic groups.

2.2.4 Determination of carboxylate content

Electric conductivity titration method was used to determine the carboxylate content of nanofibers as follow; a dried sample (50 mg) was mixed with 0.01 M HCl (15 mL) and deionized water (20 mL) with stirring. The mixture was then titrated with a solution of 0.01 M sodium hydroxide (NaOH). The carboxylate content was determined by the sudden change in conductivity [43–45].

2.2.5 Fibrillation process

The mechanical defibrillation processes were carried out through two processes to disassemble the fiber structure: (1) the low-shear mechanical defibrillation process (Ultra Turrax T-25 dispersant, IKA, Germany) with speed of 1000 rpm for 15 min at room temperature to evaluate processing efficiency on a small amount of fibers and (2) Masuko grinder (Masuko Sangyo Co., Ltd., Japan) for high quality and efficient CNFs production. The pulps with 2% solid content were rotated between two grinding stones with a velocity of 1500 rpm with

the gap distance between the rotating discs from 0 to −10 μm and the fibers were run through the grinder for about 120 min.

2.3 Characterization of CNFs

The microscopic fraction of the suspension was characterized using an optical microscope (OM) (Zeiss Axio Vert.A1, Germany). Each CNFs suspension was previously diluted to 0.1 wt%, stirred for 10 min with Ultra Turrax (IKA® T-25), and plunged for 5 min in an ultrasonic bath to foster dispersion. The pictures were taken at different magnifications and analyzed with Fiji software. Morphological characterizations of the CNFs were performed by scanning electron microscopy (SEM) using a Jeol JXA 840A system running at 5–10 keV. Before observation, the freeze dried samples were coated with gold using a sputter coater system (Edwards Sputter Coater, UK). Atomic force microscope (AFM) Multimode (DI, Veeco, Instrumentation Group) was used to characterize TOCNFs in tapping mode with multi 130 tips. Transmission electron microscopy (TEM) was carried out using a high-resolution transmission electron microscope (JEM-2100 transmission electron microscope, JEOL, Tokyo, Japan). Fourier transformed infrared (FT-IR) spectra were obtained with a Perkin Elmer FT-IR spectrometer (Perkin Elmer, USA) using KBr tablets in the range of 4000–500 cm^{-1}. X-ray diffraction (XRD) patterns were recorded using X-ray diffractometer (PANa-lytical, Netherlands) at room temperature with a monochromatic Cu Kα radiation source (λ = 1.5418 A) with a 2θ angle ranging from 4° to 60°. The crystallinity index was calculated using Segal method [46].

$$\text{Crystalinity index} = \left(1 - \frac{I_{am}}{I_{200}} \right) \tag{1}$$

where I_{200} corresponds to the maximum intensity of the crystalline peak located at 2θ = 22–23° and I_{am} is the intensity of the valley located at 2θ = 18–19° associated to the amorphous material.

Determination of the nanoscale particle quantity by a gravimetric method in suspensions was carried out according to Naderi et al. [47] A dilute CNFs suspension (0.02 wt%) was centrifuged at 1000 g for 15 min to separate the components according to their dimensions. The concentration, before and after centrifugation, was measured, and the nanosized fraction is calculated according to Eq. (2):

$$NF(w/w\%) = \left(C_{ac}/C_{bc} \right) \times 100 \tag{2}$$

where C_{ac} and C_{bc} are assigned to the mass concentration after and before centrifugation, respectively. NF (%) corresponds to the amount of TOCNFs, nanofibril aggregates, and also larger, coarser entities that have the ability to resist phase separation

through the centrifugal force. A diluted CNFs suspension (0.1 wt%) was stirred for 10 min with Ultra Turrax (IKA® T-25) firstly before measuring the turbidity with a portable turbidimeter (Aqualytic, AL-250, wavelength 860 nm). The zeta potential (mV) of 0.1 wt% aqueous CNFs suspensions was measured without ionic strength adjustment using a Zetasizer Nano S90 (Malvern Instrument). The value was calculated from the electrophoretic mobility of the suspension using Henry equation and Huckel approximation validated for $ka = 1$, where k is the inverse of Debye length and a is the nanoparticle radius [48]. Three measurements were conducted for each suspension, and the mean and standard deviation were reported.

2.4 Nanopaper preparation and characterization

Enzymatic, TEMPO, and regenerated CNFs nanopapers were prepared with a sheet former (Rapid Kothen, ISO 5269–2) from 2 g of CNFs (dry content) diluted to 0.5% in deionized water. Firstly, the suspension was filtered under vacuum at 800 mbar during a specific time until removal of water supernatant. After this time, the filtration was extended for five additional minutes. Then, the sheet was dried under vacuum at 85 °C between (from interior to exterior) two nylon sieves (one on each side) to prevent adherence and two cardboards (one on each side) for 20 min. All films were stored for 48 h in a conditioned room at 23 °C and 50% RH before characterization.

Tensile tests were performed on samples 10-cm long and 15-mm wide with a cross-head speed of 10 mm/min. The tensile properties were measured following the standard NF Q03-004 with a vertical extensometer (Instron 5965). The basis weight was measured using a surface of 65×50 mm², and thickness was then fed into the tensile device to obtain the Young's modulus. For each sample, three measurements were carried out from three different nanopapers. The tear resistance tests were carried out using a tear tester (Noviprofibre, Elmendorf pendulum 4000 mN, France) on samples of 65 and 50 mm² dimensions. The force (mN) for tear propagation was measured, and a minimum of three measurements were recorded for each sample. The prepared nanopapers were subjected to wavelength of 550 nm using a UV spectrophotometer (Shimadzu Manufacturing Inc., USA) in photometric mode to measure their transmittance. For each sample, two nanopapers were analyzed for a total of 6 measurements, with an average calculated.

The porosity was calculated from the nanopaper basis weight (g/m²) and its thickness (μm), using the following equation (Eq. (3)) [41]:

$$P(\%) = 1 - BW(e \times \rho_c) \tag{3}$$

where BW is the basis weight (kg/m²), e is the thickness (m), and ρ_c is the density of cellulose, taken as 1540 kg/m³. In this test, the more homogeneous the fibers are at the

nanoscale, the more cohesive the material will be, and the lower the porosity. At least five replicates were performed.

The water vapor permeability (WVP) of the prepared nanopapers was determined according to Tunc et al. [49]. The WVP value was gravimetrically determined at 20 °C using a modified (ASTM Standards, 1995) procedure. Samples (discs 40 mm in diameter) were sealed tightly with Teflon seals and silicone grease in a glass permeation cell containing 5 g of anhydrous calcium chloride as desiccant (0% RH). The permeation cell was placed at 20 °C in desiccators containing a saturated potassium sulfate solution (97% RH). The cells were weighed on an analytical balance every hour during the first 6 h and then every 24 h for 7 days. At least three samples of each type of nanopapers were tested, and WVP was evaluated from the slope of the mass gain versus time curve as follows (Eq. (4)):

$$WVP\left(\mathrm{gm^{-1}S^{-1}Pa^{-1}}\right) = wx/A\Delta t\Delta p \tag{4}$$

where w is the slope of the weight loss versus time (g s⁻¹), x is the nanopaper thickness (mm), Δt is the time of weight loss (s), A is the area of exposed nanopaper (mm²), and Δp is the partial water vapor pressure difference across the samples corresponding to 0–97% RH, i.e., 1875 Pa.

2.5 Energy measurement

The super-grinding treatment is used to determine energy consumption. The Masuko device was equipped with a three-phase wattmeter that measured the active power directly. During the 2.5 h of treatment, the variations in power were meticulously recorded at a rate of one measurement per minute. The specific energy consumption in kWh/kg is calculated as follows:

$$ESP(\mathrm{kWh/kg}) = \left(\left(P_i - P_o\right) * t_i\right)/m_i \tag{5}$$

where P_i = average power consumption, P_o = no load power, t_i = grinding time in hours, and m_i = mass of oven dried raw material in kg.

2.6 Quality index (QI)

As a tool to compare the quality of CNFs suspensions, an equation regrouping 5 test values was used, adapted from the publication of Desmaisons et al. [50]. The obtained value named QI is representative of the global quality of CNFs suspensions in terms of optical and mechanical properties.

The adapted equation used for the QI calculation is shown below (Eq. (6)):

$$QI = 2 \, x \, turbidity \, mark \; + \; 1 \, x \, transmittance \, mark \; + \; 2 \, x \, tear \, resistance \, mark$$
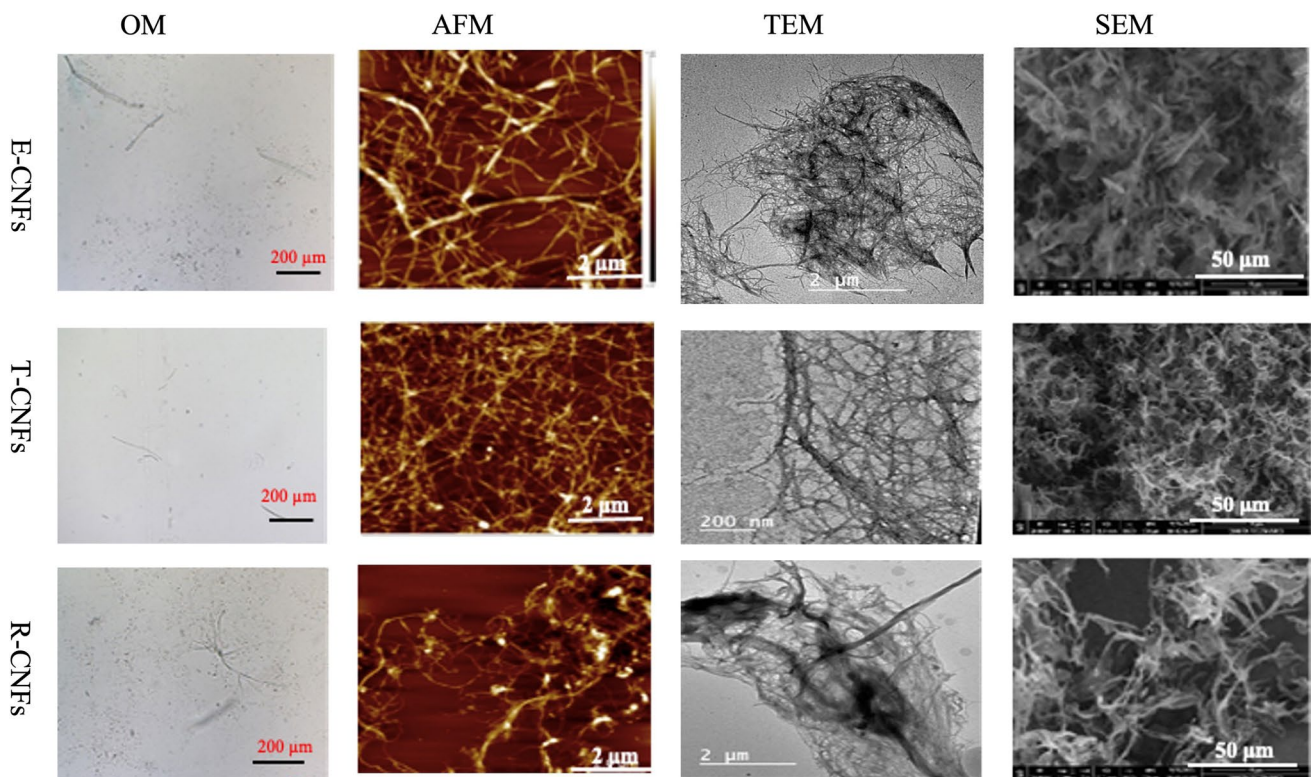$$+ \; 2 \, x \, Young's \, modulus \, mark \; + \; 2 \, x \, porosity \, mark \; + \; 1\pi \tag{6}$$

Fig. 1 Optical microscopy (OM), atomic force microscopy (AFM), transmission electron microscopy (TEM), and scanning electron microscopy (SEM) images for CNFs prepared from cellulose I enzymatically pretreated (E-CNFs), TEMPO pretreated (T-CNFs), and cellulose II (R-CNFs)

where marks are calculated from raw test values as indicated in the original publication. The resulting equation including the raw test values is shown below (Eq. (7)):

$$QI = -0.02 \times x1 + 1.65 \times In\ (x2) - 7.18 \times In\ (x3) \\ - 0.07 \times x4^2 + 2.54 \times x4 - 0.32 \times x5 + 89.96 \tag{7}$$

where $\times 1$ is the turbidity (NTU), $\times 2$ is the transmittance (%), $\times 3$ is the tear resistance (mN), $\times 4$ is the Young's modulus (GPa), and $\times 5$ is the porosity (%).

3 Results and discussions

In order to develop and expand the feasibility of producing CNFs from available agricultural wastes, different chemical and physical methods were implemented, and, as a result, CNFs with different degrees of fibrillation were produced to meet the recent requirements of versatile applications. In terms of effectiveness and eco-friendliness, CNFs can be easily prepared from bleached bagasse pulp, rather than from wood fibers or highly processed and degraded industrial wood byproducts, via dissolution and regeneration using NMMO. Cellulose chains can adopt an anti-parallel arrangement of stable crystal type known as cellulose II upon dissolution in NMMO and regeneration of cellulose I [51] exhibiting a reorganized inter- and intra- hydrogen bonding pattern [40]. The mentioned changes may impact the properties of the resulting suspension. Figure 1 shows OM, AFM, TEM, and SEM images for enzymatic CNFs (E-CNFs), TEMPO-oxidized CNFs (T-CNFs), and regenerated CNFs (R-CNFs). All the mentioned CNFs exhibit a strongly entangled branched network of fibrous structure. A previous study reported that partial chain degradation and oxidation of C_1 -OH to onic acid accompanied the dissolution of cellulose in NMMO [33]. The induced carboxylic groups can enhance the fibrillation of the regenerated cellulose. Generally, the effectiveness of nanofibrillation is evaluated with the presence or absence of few residual fragments and/or microfibers observed by optical microscopy. The optical microscope image for T-CNFs is clear due to its good nanofibrillation, while those for E-CNFs and R-CNFs show very few aggregates. The aggregates for R-CNFs may be due to the presence of some microfibers. A network structure of nano- and micrometric criteria was observed for R-CNFs as can be seen in the SEM image, which shows a dense network of some agglomerated structure due to the hydrophobic interactions ascribed to the amphiphilic nature of cellulose,

arised due to conversion to cellulose II, rather than hydrogen bonding of the regenerated cellulose after dissolution, where the dissolution and regeneration of cellulose lead to the reorganization of the intra- and inter-molecular hydrogen bonds [52]. The AFM and TEM observations highlight the formation of nanofibers with an average effective diameter less than 100 nm and with several micrometers in length. FTIR spectroscopy can be used to identify the effect of the different pretreatments on the chemical composition of CNFs. The FTIR spectra for E-CNFs, T-CNFs, and R-CNFs are displayed in Fig. 2. For all samples, a characteristic peak around 3300 cm^{-1} is ascribed to the stretching of OH group of cellulose. However, a broader peak was detected for R-CNFs due to stronger inter- and intra-hydrogen bonds that shifted the peak to higher wave umbers. All spectra exhibit a transmittance peak at about 2800 cm^{-1} attributed to C-H and in the range 1600–1650 cm^{-1} corresponding to the C-O stretching vibration. The very low intensity of the former peak for E-CNFs may be attributed to the breaking action of the endoglucanase enzyme at this site. The spectrum of T-CNFs shows a characteristic C=O band at 1740 cm^{-1} assigned to the carbonyl group resulting from TEMPO oxidation.
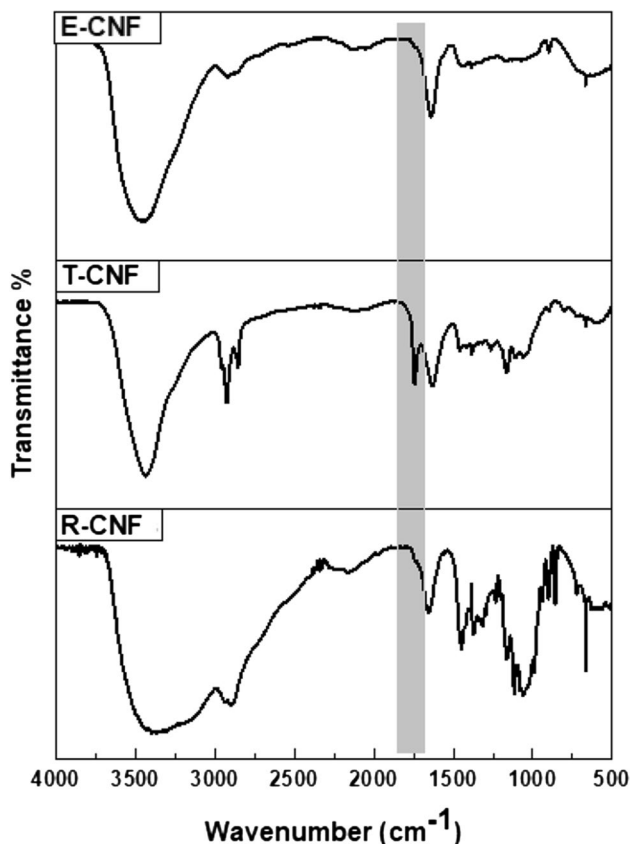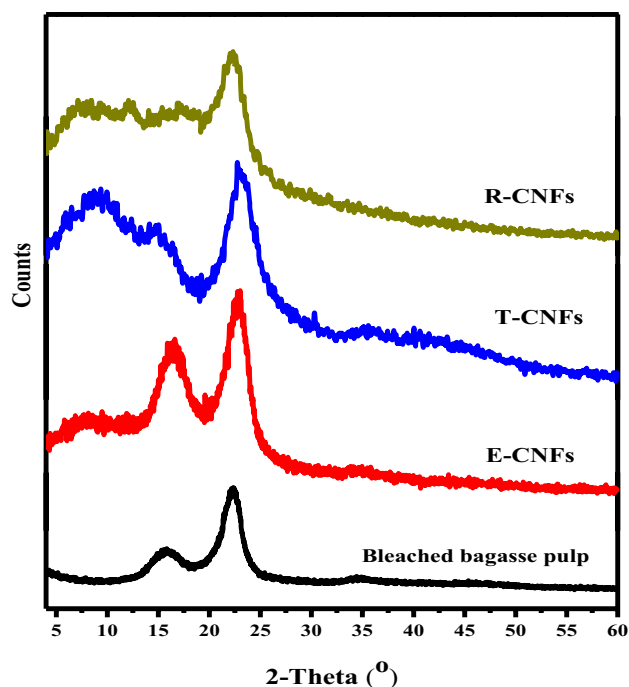

Fig. 3 XRD patterns for bleached bagasse pulp, E-CNFs, T-CNFs, and R-CNFs

The crystalline structure of E-CNFs, T-CNFs, and R-CNFs was assessed using X-ray diffraction (XRD) shown in Fig. 3. The diffraction patterns for E-CNFs and T-CNFs are typical of cellulose Iβ structure with diffraction peaks at 2θ = 15.5°, 16.8°, and 22.5°, which correspond to (11̄0), (110), and (200) crystallographic planes, respectively. The diffraction pattern for R-CNFs indicates the cellulose II crystalline structure with doublet 2θ values (19.8° and 22.7°) attributed to (110) and (020) planes [33]. The crystallinity index calculated from Eq. (1) was 69%, 74%, and 63% for E-CNF, T-CNFs, and R-CNFs, respectively. The value of the crystallinity index for bleached bagasse pulp was found to be 54.5%. Disordering and defect of the cellulose structure due to dissolution and regeneration followed by fibrillation impacted the crystallinity of R-CNFs resulted in a lower crystallinity compared to E-CNFs and T-CNFs. The low crystallinity of the regenerated cellulose may be related to NMMO crystallization during cooling of the cellulose/NMMO mixture [53].

The zeta potential (ζ) values for E-CNFs, T-CNFs, and R-CNFs were − 21, − 59, and − 35 mV, respectively. These negative values confirm the presence of surface charge for CNFs under investigation, regardless of the type of pretreatment. However, the influence of enzymatic treatment on the charge is weak, while the influence of TEMPO oxidation is significant as expected. Dissolution and regeneration of cellulose fibers from NMMO solvent resulted in moderate charge value due to introduction of carbocyclic acid group

Fig. 2 FTIR spectra for E-CNFs, T-CNFs, and R-CNFs

Fig. 4 Photographs of CNFs suspensions at a concentration of 1 wt%
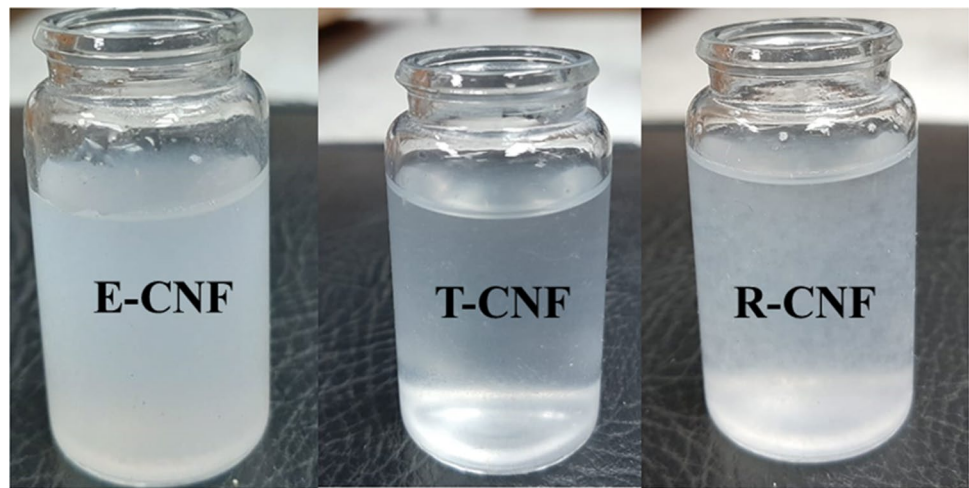
at the chain end (C1–COOH) [33]. T-CNFs possesses a surface charge of 1.9 mml/g and a ζ value of -59 mV, i.e., 1.6-fold the value observed for R-CNFs, which clearly indicate higher amount of negative charges created by TEMPO oxidation rather than dissolution in NMMO solvent. This difference in surface charge affects properties such as stability of the suspension. For nanofibrillated cellulose (cellulose II) prepared by [54] using 48 wt% sulfuric acid to hydrolyze mercerized wood pulp, the ζ value was not detectable due to the instability of the suspension in contrast to R-CNFs, as the stability of the suspension was promoted by the carboxylic groups introduced during the dissolution step as shown in Fig. 4. The R-CNFs suspension was homogeneous and stable, white in color with traces of fragmented fibers, and turbid in appearance, compared with T-CNFs at the same concentration. The stability of the suspension was detected for two days; the concentration was selected according to Mei-Chun et al. (2014) [55]. Also, this concentration was chosen on the basis of being less than 2% (the concentration of the suspension for defibrillation). On the other hand, the carboxylate content of T-CNFs, E-CNFs, and R-CNFs, respectively, was determined to be 0.9, 0.18, and 0.14 mmol/g. The carboxyl group raised the surface charge of the CNFs, resulting in T-CNFs having greater dispersion properties than E-CNFs and R-CNFs. As a result, the suspension of CNFs may remain constant with less flocculation.

To characterize the optical properties of the CNFs suspensions, their turbidity was assessed. Turbidity is one of the optical parameters used to determine the quality of nanosized materials. It is the haziness or opacity of a suspension of individual invisible suspended particles due to attenuation of light passing through the suspension. Turbidity results for the different CNFs are included in Table 1. T-CNFs exhibits the lowest value (160 NTU) due to the destructive effect of TEMPO oxidation on the cellulosic fibers to the nano-dimension, and the value observed for E-CNF (272

Table 1 Optical and mechanical properties for cellulose nanofibrils in suspension or as nanopapers, and their associated quality index

	E-CNFs	T-CNFs	R-CNFs
Nanosized fraction (%)	72 ± 5.7	77.5 ± 6.2	68.5 ± 4.5
Transmittance (%)	12.5 ± 0.6	25 ± 1.1	7.5 ± 0.4
Tear resistance (mN)	17.5 ± 25	5.5 ± 0.2	20 ± 2.1
Young's modulus (GPa)	7.3 ± 1.1	10.3 ± 1.3	6.9 ± 0.6
Porosity (%)	30 ± 2.1	35 ± 3.5	35.6 ± 2.7
Turbidity (NTU)	272 ± 22	160 ± 18	315 ± 15.3
Quality index	74.5 ± 2.2	84.2 ± 1.6	68.3 ± 1.2

NTU) agrees with that reported by Banvillet et al. [41] (242 NTU). R-CNFs showed the highest value (315 NTU) among the tested CNFs. However, it is comparable to the values obtained for fibers subjected to two pretreatments (enzymatic and alkali) prior to fibrillation step (314 NTU) [41].

Further assessment of R-CNFs was conducted via the fabrication of paper sheets to conclude and have a complete visualization of the feasibility of using the cellulose regeneration concept in medical and packaging applications. The average UV transmittance values for CNFs are presented in Table 1. R-CNFs showed the lowest transmission value compared to T-CNFs or even E-CNFs. Among the factors affecting the light transmittance is the particle size [56]. This result is confirmed by another test, the nanosized fraction (Table 1). The significant difference in this value may be due to the fact that the particle size has a stronger effect on the transmitted light for cellulose II than for cellulose I [14, 54]. Figure 5 shows the aspect of the different nanopapers. A slight difference in transparency is observed between all nanopapers, and the details of the pictures are clear for all images. Regarding haziness of R-CNFs nanopaper exhibits the lowest due to agglomeration previously discussed in SEM section.

Fig. 5 Aspect of nanopapers prepared from E-CNFs, T-CNFs, and R-CNFs
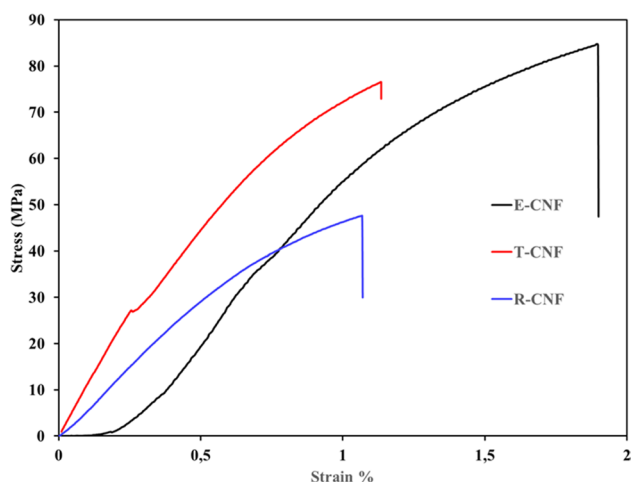

Fig. 6 Typical stress–strain curves for E-CNFs, T-CNFs, and R-CNFs nanopapers

Despite of the rapid progress in the preparation and characterizations of CNFs, the evaluation of their quality remains a challenge [57, 58]. Desmaisons et al. [50] suggested a multicriterion method based on the guidelines of a quality index calculation for nanofiber cellulose suspensions as a new tool to monitor their production. The QI values for the samples under investigation are shown in Table.1. They were found to be 74.5, 84.2, and 68.3 for E-CNFs, T-CNFs, and R-CNFs, respectively. T-CNFs has the highest quality index, followed by E-CNFs, while the enzymatically pretreated CNFs have a value of 73.1 [50]. Whereas the quality index value for R-CNFs seems to be lower than E-CNFs and T-CNFs, nevertheless it appears to be higher than that of many commercial CNFs and cellulose nanofibers obtained through various treatments; treatments include ultrafine friction grinding (59.5), twin-screw extrusion (54.9), and high-pressure homogenization (64.2) [50, 59].

Typical stress–strain curves obtained for nanopapers prepared from E-CNFs, T-CNFs, and R-CNFs are presented in Fig. 6. For the enzymatically pretreated nanopaper, the

average tensile strength was 84 ± 1.5 MPa, and the average strain at break was 1.8%, while lower tensile strength (76 ± 2.0 MPa) and strain at break (1.12%) values were obtained for the nanopaper prepared from TEMPO-oxidized CNFs. An even more pronounced decrease in tensile strength (48 ± 2.5 MPa) and strain at break (1.06%) is noticed for the nanopaper prepared from R-CNFs most probably due to the heterogeneous diameter of micro- and nanofibers previously observed. The relatively high strength of E-CNFs is due to the less aggressive hydrolysis treatment which was found to keep the high aspect ratio of cellulose I [20] in contrary to cellulose II with its characteristic feature of antiparallel glucan chains which typically has reduced strength [60].

Moreover, in addition to the characteristics required to evaluate and calculate the quality index of the prepared NFCs, energy consumption and water vapor permeability were measured to provide a clear vision of R-CNFs.

3.1 Energy consumption

The evolution of the energy consumption upon grinding cycles for the three materials is presented in Fig. 7. For all materials, the energy consumptions increased almost linearly with the increase of cycles number, with an energy consumption rate of ca. 0.6, 0.3, and 0.4 kWh/kg per grinding cycle for T-CNFs, E-CNFs, and R-CNFs respectively. The total energy consumption for T-CNFs, E-CNFs, and R-CNFs were found to be 5.0 kWh/kg, 6.2 kWh/kg, and 8.7 kWh/kg respectively. The relatively high energy consumed in case of R-CNFs is due to the high number of cycles needed to accomplish fibrillation despite of the low energy consumed per cycle.

The evolution of the water vapor permeability of the different nanopapers as a function of time was evaluated, and the results are presented in Fig. 8. The very close behavior for all CNFs may be ascribed to the almost similar organization of the nanofibers within the nanopaper which seem to enhance and regulate the barrier properties of the material. At the beginning of the experiment, very close WVP values were

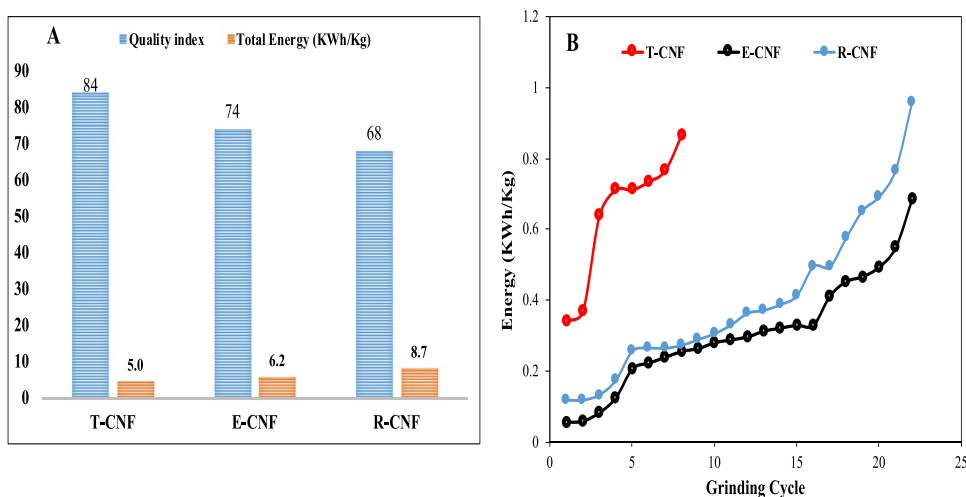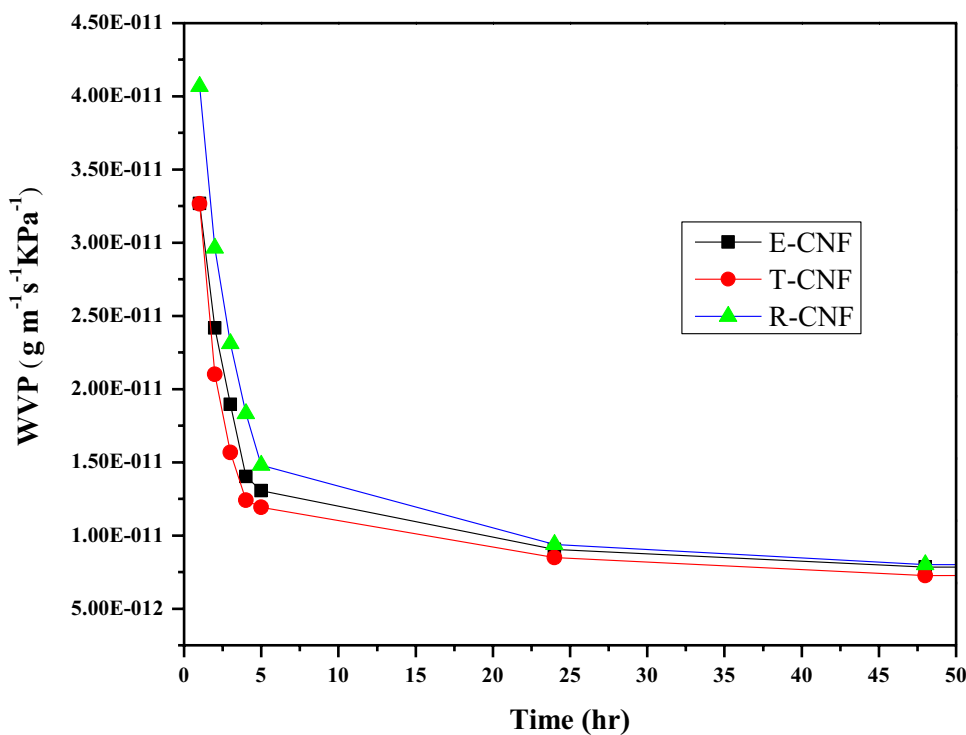**Fig. 7** Evaluation of different CNFs produced according to (**A**) relative quality index (**B**) Relative energy consumed

Fig. 8 Evolution of the water vapor permeability of the nanopapers over time

obtained, i.e., 3.28×10^{-11} and 3.26×10^{-11} (g m^{-1} s^{-1} kPa^{-1}) for T-CNFs and E-CNFs nanopapers, respectively, while this value was slightly higher for R-CNFs nanopaper (4.06×10^{-11} g m^{-1} s^{-1} kPa^{-1}). A rapid decrease in the WVP value was observed for all the nanopapers during the first 5 h, and the values reached 1.30×10^{-11}, 1.19×10^{-11}, and 1.48×10^{-11} (g m^{-1} s^{-1} kPa^{-1}) for E-CNFs, T-CNFs, and R-CNFs nanopapers, respectively. The slightly higher WVP values reported for R-CNF may be ascribed to the relatively open network structure of the network compared to E-CNFs and T-CNFs. The WVP values continue to decrease up to 24 h and then stabilize at a plateau until the end of the measurements (7 days);

the data shown in Fig. 7 corresponding to the first 48 h. A more prominent influence of nanoporosity and entanglement rather than crystallinity on WVP of nanofibrillated cellulose was reported, which is in agreement with our CNFs of very close porosity and entanglement [61].

4 Conclusions

Cellulose nanofibers have been successfully prepared from cellulose II (R-CNFs) obtained by dissolution of bleached bagasse pulp in N-methylmorpholine N-oxide solution and regeneration

by using water as a precipitant. Their characteristics and properties have been assessed and compared to those obtained for cellulose nanofibers prepared from enzymatically (E-CNFs) or TEMPO-oxidation (T-CNFs) pretreated native bleached bagasse pulp. The stability of the R-CNFs suspension was evaluated using zeta potential measurement. Optical microscopy observation of R-CNFs suspension indicated the presence of some residual fragments. R-CNFs nanopaper characteristics were of reasonable properties when compared to nanopapers prepared from E-CNFs or T-CNFs despite of lower crystallinity. The effectiveness of the fibrillation was estimated through the quality index. A value of 68.3 was obtained for R-CNFs, which is higher than the majority of industry reference CNFs quality indices, and close to the quality index observed for E-CNFs (74.5), indicating that the diameter of the nanofibers is less than 50 nm after the fibrillation process. The porosity and water vapor permeability are also very close to the values observed for E-CNFs and T-CNFs. The dispersion of R-CNFs exhibits a gel-like feature at very low concentration 1% that afford the potential to be used in biomedical applications due to its entangled network in addition to easy, eco-friendly, and safe dissolution in NMMO and regeneration.

Declarations

Conflict of interest The authors declare no competing interests.

References

1. Himmel ME, Ding SY, Johnson DK et al (2007) Biomass recalcitrance: engineering plants and enzymes for biofuels production. Science 315:804–807

2. Kamel R, El-Wakil NA, Dufresne A, Elkasabgy NA (2020) Nanocellulose: from an agricultural waste to a valuable pharmaceutical ingredient. Int J Biol Macromol 163:1579–1590

3. Hassan ML, Mathew AP, Hassan EA et al (2012) Nanofibers from bagasse and rice straw: process optimization and properties. Wood Sci Technol 46:193–205. https://doi.org/10.1007/s00226-010-0373-z

4. Abouzeid RE, Khiari R, Beneventi D, Dufresne A (2018) Biomimetic mineralization of three-dimensional printed alginate/TEMPO-oxidized cellulose nanofibril scaffolds for bone tissue engineering. Biomacromol 19:4442–4452. https://doi.org/10.1021/acs.biomac.8b01325

5. Abouzeid RE, Khiari R, El-Wakil N, Dufresne A (2019) Current state and new trends in the use of cellulose nanomaterials for wastewater treatment. Biomacromol 20:573–597

6. Abouzeid RE, Khiari R, Salama A et al (2020) In situ mineralization of nano-hydroxyapatite on bifunctional cellulose nanofiber/polyvinyl alcohol/sodium alginate hydrogel using 3D printing. Int J Biol Macromol 160:538–547. https://doi.org/10.1016/j.ijbiomac.2020.05.181

7. Hassan ML, Fadel SM, Abouzeid RE et al (2020) Water purification ultrafiltration membranes using nanofibers from unbleached and bleached rice straw. Sci Rep 10(1). https://doi.org/10.1038/s41598-020-67909-3

8. Abdul Khalil HPS, Davoudpour Y, Islam MN et al (2014) Production and modification of nanofibrillated cellulose using various mechanical processes: a review. Carbohyd Polym 99:649–665

9. Hassan M, Abou-Zeid R, Hassan E et al (2017) Membranes based on cellulose nanofibers and activated carbon for removal of *Escherichia coli* bacteria from water. Polymers 9(8):335. https://doi.org/10.3390/polym9080335

10. Hassan E, Hassan M, Abou-zeid R et al (2017) Use of bacterial cellulose and crosslinked cellulose nanofibers membranes for removal of oil from oil-in-water emulsions. Polymers 9(9):388. https://doi.org/10.3390/polym9090388

11. Dufresne A (2013) Nanocellulose: a new ageless bionanomaterial. Mater Today 16:220–227

12. Santucci BS, Bras J, Belgacem MN et al (2016) Evaluation of the effects of chemical composition and refining treatments on the properties of nanofibrillated cellulose films from sugarcane bagasse. Ind Crops Prod 91:238–248. https://doi.org/10.1016/j.indcrop.2016.07.017

13. Lahtinen P, Liukkonen S, Pere J et al (2014) A Comparative study of fibrillated fibers from different mechanical and chemical pulps. BioResources 9:2115–2127. https://doi.org/10.15376/biores.9.2.2115-2127

14. Rezayati Charani P, Dehghani-Firouzabadi M, Afra E et al (2013) Production of microfibrillated cellulose from unbleached kraft pulp of Kenaf and Scotch Pine and its effect on the properties of hardwood kraft: Microfibrillated cellulose paper. Cellulose 20:2559–2567. https://doi.org/10.1007/s10570-013-9998-z

15. Chen W, Yu H, Liu Y et al (2011) Individualization of cellulose nanofibers from wood using high-intensity ultrasonication combined with chemical pretreatments. Carbohyd Polym 83:1804–1811. https://doi.org/10.1016/j.carbpol.2010.10.040

16. Chakraborty A, Sain M, Kortschot M (2005) Cellulose microfibrils: a novel method of preparation using high shear refining and cryocrushing. Holzforschung 59:102–107. https://doi.org/10.1515/HF.2005.016

17. Qing Y, Sabo R, Zhu JY et al (2013) A comparative study of cellulose nanofibrils disintegrated via multiple processing approaches. Carbohyd Polym 97:226–234. https://doi.org/10.1016/j.carbpol.2013.04.086

18. Mishra SP, Manent AS, Chabot B, Daneault C (2012) Production of nanocellulose from native cellulose - various options utilizing ultrasound. BioResources 7:422–435. https://doi.org/10.15376/biores.7.1.0422-0436

19. Henriksson M, Henriksson G, Berglund LA, Lindström T (2007) An environmentally friendly method for enzyme-assisted preparation of microfibrillated cellulose (MFC) nanofibers. Eur Polymer J 43:3434–3441. https://doi.org/10.1016/j.eurpolymj.2007.05.038

20. Pääkko M, Ankerfors M, Kosonen H et al (2007) Enzymatic hydrolysis combined with mechanical shearing and high-pressure homogenization for nanoscale cellulose fibrils and strong gels. Biomacromol 8:1934–1941. https://doi.org/10.1021/bm061215p

21. Saito T, Nishiyama Y, Putaux JL et al (2006) Homogeneous suspensions of individualized microfibrils from TEMPO-catalyzed oxidation of native cellulose. Biomacromol 7:1687–1691. https://doi.org/10.1021/bm060154s

22. https://www.sigmaaldrich.com/catalog/product/aldrich/214000?lang=en&region=SE (accessed Dec 27, 2019).

23. Lavoine N, Desloges I, Dufresne A, Bras J (2012) Microfibrillated cellulose - its barrier properties and applications in cellulosic materials: a review. Carbohyd Polym 90:735–764

24. Taha M, Hassan ML, Dewidare M et al (2021) Evaluation of eco-friendly cellulose and lignocellulose nanofibers from rice straw using multiple quality index. Egyp J Chem 64:4707–4717. https://doi.org/10.21608/ejchem.2021.77618.3800

25. Abdul Khalil HP, Davoudpour Y, Bhat AH et al (2015) Electrospun cellulose composite nanofibers. In: Handbook of polymer nanocomposites. Processing, performance and application: Volume C: Polymer nanocomposites of cellulose nanoparticles. Springer, Heidelberg, pp 191–228

26. Ye D, Lei X, Li T et al (2019) Ultrahigh tough, super clear, and highly anisotropic nanofiber-structured regenerated cellulose films. ACS Nano 13:4843–4853. https://doi.org/10.1021/acsnano.9b02081

27. Yokota S, Kitaoka T, Opietnik M et al (2008) Synthesis of gold nanoparticles for in situ conjugation with structural carbohydrates. Angew Chem Int Edit 47:9866–9869. https://doi.org/10.1002/anie.200803922

28. Beaumont M, Rennhofer H, Opietnik M et al (2016) Nanostructured cellulose II gel consisting of spherical particles. ACS Sustain Chem Eng 4:4424–4432. https://doi.org/10.1021/acssuschemeng.6b01036

29. Freudenberg U, Zschoche S, Simon F et al (2005) Covalent immobilization of cellulose layers onto maleic anhydride copolymer thin films. Biomacromol 6:1628–1634. https://doi.org/10.1021/bm0492529

30. Li HJ, Cao YM, Qin JJ et al (2006) Development and characterization of anti-fouling cellulose hollow fiber UF membranes for oil-water separation. J Membr Sci 279:328–335. https://doi.org/10.1016/j.memsci.2005.12.025

31. Liebner F, Potthast A, Rosenau T et al (2008) Cellulose aerogels: highly porous, ultra-lightweight materials. Holzforschung 62:129–135. https://doi.org/10.1515/HF.2008.051

32. Kim CW, Kim DS, Kang SY et al (2006) Structural studies of electrospun cellulose nanofibers. Polymer 47:5097–5107. https://doi.org/10.1016/j.polymer.2006.05.033

33. Zimmermann R, Müller Y, Freudenberg U et al (2016) Oxidation and structural changes in NMMO-regenerated cellulose films. Cellulose 23:3535–3541. https://doi.org/10.1007/s10570-016-1084-x

34. Kabir MM, Niklasson C, Taherzadeh MJ, Horváth IS (2014) Biogas production from lignocelluloses by N-methylmorpholine-N-oxide (NMMO) pretreatment: effects of recovery and reuse of NMMO. Biores Technol 161:446–450. https://doi.org/10.1016/j.biortech.2014.03.107

35. Kuo CH, Lee CK (2009) Enhanced enzymatic hydrolysis of sugarcane bagasse by N-methylmorpholine-N-oxide pretreatment. Biores Technol 100:866–871. https://doi.org/10.1016/j.biortech.2008.07.001

36. Chou W-T, Lai M-Y, Huang K-S (2011) Method of recovering aqueous N-methylmorpholine-N-oxide solution used in production of lyocell fiber. Us 2011/0226427 a1 1. Pub. No.: US 2011/0226427 A1. Pub. Date: Sep. 22, 2011

37. Sirviö JA, Visanko M, Liimatainen H (2015) Deep eutectic solvent system based on choline chloride-urea as a pre-treatment for nanofibrillation of wood cellulose. Green Chem 17:3401–3406. https://doi.org/10.1039/c5gc00398a

38. Yu W, Wang C, Yi Y et al (2020) Comparison of deep eutectic solvents on pretreatment of raw ramie fibers for cellulose nanofibril production. ACS Appl Mater Interfaces. https://doi.org/10.1021/acsomega.0c00506

39. Li P, Sirviö JA, Haapala A, Liimatainen H (2017) Cellulose nanofibrils from nonderivatizing urea-based deep eutectic solvent pretreatments. ACS Appl Mater Interfaces 9:2846–2855. https://doi.org/10.1021/acsami.6b13625

40. Krysztof M, Olejnik K, Kulpinski P et al (2018) Regenerated cellulose from N-methylmorpholine N-oxide solutions as a coating agent for paper materials. Cellulose 25:3595–3607. https://doi.org/10.1007/s10570-018-1799-y

41. Banvillet G, Depres G, Belgacem N, Bras J (2021) Alkaline treatment combined with enzymatic hydrolysis for efficient cellulose nanofibrils production. Carbohydr Polym 255:117383. https://doi.org/10.1016/j.carbpol.2020.117383

42. Saito T, Isogai A (2006) Introduction of aldehyde groups on surfaces of native cellulose fibers by TEMPO-mediated oxidation. Colloids Surf, A 289:219–225. https://doi.org/10.1016/j.colsurfa.2006.04.038

43. Abou-Zeid RE, Dacrory S, Ali KA, Kamel S (2018) Novel method of preparation of tricarboxylic cellulose nanofiber for efficient removal of heavy metal ions from aqueous solution. Int J Biol Macromol 119:207–214. https://doi.org/10.1016/j.ijbiomac.2018.07.127

44. da Silva PD, Montanari S, Vignon MR (2003) TEMPO-mediated oxidation of cellulose III. Biomacromol 4:1417–1425. https://doi.org/10.1021/bm034144s

45. Fukuzumi H, Saito T, Okita Y, Isogai A (2010) Thermal stabilization of TEMPO-oxidized cellulose. Polym Degrad Stab 95:1502–1508. https://doi.org/10.1016/j.polymdegradstab.2010.06.015

46. Segal L, Creely JJ, Martin AE, Conrad CM (1959) An empirical method for estimating the degree of crystallinity of native cellulose using the X-ray diffractometer. Text Res J 29:786–794. https://doi.org/10.1177/004051755902901003

47. Naderi A, Lindström T, Sundström J (2015) Repeated homogenization, a route for decreasing the energy consumption in the manufacturing process of carboxymethylated nanofibrillated cellulose? Cellulose 22:1147–1157. https://doi.org/10.1007/s10570-015-0576-4

48. Uetani K, Yano H (2012) Zeta potential time dependence reveals the swelling dynamics of wood cellulose nanofibrils. Langmuir 28:818–827. https://doi.org/10.1021/la203404g

49. Tunc S, Angellier H, Cahyana Y et al (2007) Functional properties of wheat gluten/montmorillonite nanocomposite films processed by casting. J Membr Sci 289:159–168. https://doi.org/10.1016/j.memsci.2006.11.050

50. Desmaisons J, Boutonnet E, Rueff M et al (2017) A new quality index for benchmarking of different cellulose nanofibrils. Carbohyd Polym 174:318–329. https://doi.org/10.1016/j.carbpol.2017.06.032

51. Kolpak FJ, Blackwell J (1976) Determination of the structure of cellulose II. Macromolecules 9:273–278. https://doi.org/10.1021/ma60050a019

52. Lindman B, Medronho B (2015) The subtleties of dissolution and regeneration of cellulose: breaking and making hydrogen bonds. BioResources 10:3811–3814

53. El-Wakil NA, Hassan ML (2008) Structural changes of regenerated cellulose dissolved in FeTNa, NaOH/thiourea, and NMMO systems. J Appl Polym Sci 109:2862–2871. https://doi.org/10.1002/app.28351

54. Han J, Zhou C, Wu Y et al (2013) Self-assembling behavior of cellulose nanoparticles during freeze-drying: effect of suspension

concentration, particle size, crystal structure, and surface charge. Biomacromol 14:1529–1540. https://doi.org/10.1021/bm4001734

55. Li MC, Wu Q, Song K et al (2015) Cellulose nanoparticles: structure-morphology-rheology relationships. ACS Sustain Chem Eng 3:821–832. https://doi.org/10.1021/acssuschemeng.5b00144

56. Tang C, Liu H (2008) Cellulose nanofiber reinforced poly(vinyl alcohol) composite film with high visible light transmittance. Compos A Appl Sci Manuf 39:1638–1643. https://doi.org/10.1016/j.compositesa.2008.07.005

57. Foster EJ, Moon RJ, Agarwal UP et al (2018) Current characterization methods for cellulose nanomaterials. Chem Soc Rev 47:2609–2679

58. Kangas H, Lahtinen P, Sneck A et al (2014) Characterization of fibrillated celluloses. A short review and evaluation of characteristics with a combination of methods. Nord Pulp Pap Res J 29:129–143. https://doi.org/10.3183/npprj-2014-29-01-p129-143

59. Espinosa E, Rol F, Bras J, Rodríguez A (2020) Use of multi-factorial analysis to determine the quality of cellulose nanofibers: effect of nanofibrillation treatment and residual lignin content. Cellulose 27:10689–10705. https://doi.org/10.1007/s10570-020-03136-3

60. Atalla RH, VanderHart DL (1984) Native cellulose: a composite of two distinct crystalline forms. Science 223:283–285. https://doi.org/10.1126/science.223.4633.283

61. Belbekhouche S, Bras J, Siqueira G et al (2011) Water sorption behavior and gas barrier properties of cellulose whiskers and microfibrils films. Carbohyd Polym 83:1740–1748. https://doi.org/10.1016/j.carbpol.2010.10.036